Development of Porous Material and Hybrid Porous Ti6Al4V Dental Implants using Metal Injection Molding (MIM)

Sugeng Supriadi[*], Ana Wilda Widiantoro, Daniel Jones
Departemen Teknik Mesin, Universitas Indonesia, Depok, INDONESIA
[*]sugeng@eng.ui.ac.id

Muhammad Faiq Zuhdi
Departemen Teknik Metalurgi dan Material, Universitas Indonesia, Depok, INDONESIA

ABSTRACT

Dental implants are biomaterial devices implanted in the jawbone through surgery to replace missing teeth. The surface topography of dental implants with surface roughness and a porous layer made of Ti6Al4V material is recommended to improve osseointegration and induce the growth of new bone tissue (bone ingrowth) while reducing the effect of stress shielding due to the high Young's modulus of the implant material. This study presents the fabrication of porous layers, the development of dental implant design, and the manufacturing process of hybrid porous dental implants using Metal Injection Molding (MIM). Surface analysis was performed on the combination of the implant core material with the porous Ti6AL4V material after the sintering process using a temperature of 1150 °C with holding times of 60, 90, and 120 minutes under an argon atmosphere with a flow rate of 1 liter/minute. The research results showed that the sintering holding time affected the percentage of porosity and hardness of the Ti6Al4V material. Surface roughness greatly influenced the shear bond strength on the surface. The higher the surface roughness value, the higher the shear bond strength. In this study, the highest shear stress value obtained was 1.54 MPa at a surface roughness (Ra) of 2.37 µm. The green part of the hybrid porous dental implant was successfully made using MIM with a mold temperature of 180 °C.

Keywords: *Dental Implants; Titanium Ti6Al4V; Hybrid Porous Dental Implant; Metal Injection Molding; Shear Bond Strength*

ISSN 1823-5514, eISSN 2550-164X

https://doi.org/10.24191/jmeche.v21i1.25362

Received for review: 2023-01-15
Accepted for publication: 2023-09-25
Published: 2024-01-15

Introduction

A dental implant is an engineered device made of biomaterials that is implanted into the jawbone through a surgical process to support the implant structure. It is considered as a replacement of tooth crown used to replace missing teeth [1]. To maintain implant performance, the most important indicator is implant stability, which consists of primary (mechanical stability) and secondary (osseointegration/ biological stability) stability. Primary stability refers to the strength of the implant's attachment to the bone that comes into mechanical contact, such as friction, whereas secondary stability is the result of the growth of new bone cells around the implant, resulting in osseointegration [2]. Factors that affect primary stability include the quantity and quality of the jawbone, surgical techniques, and the design of the dental implant. Meanwhile, secondary stability is influenced by bone modeling, dental implant, and loading conditions [3]-[4].

The failure of dental implants can occur due to inadequate osseointegration and peri-implantitis, which are influenced by patient conditions, such as poor bone density, reduced jawbone volume, the number of the patient's natural teeth, oral hygiene, smoking, bruxism, diseases like osteoporosis and diabetes [5]. Therefore, to stimulate osseointegration and prevent peri-implantitis, modifications to the surface of dental implants are necessary [6]-[7]. The modifications to implant surface topography include macro-scale modifications that depict the geometry of dental implants, micro-scale modifications that depict surface roughness (1-100 μm), and nano-scale modifications that depict surface roughness at a nanoscale (1-100 nm), which affect the interaction of cells with the implant to stimulate new bone growth [5]-[8].

The Ti6Al4V material has mechanical properties that are similar to bone, namely low elasticity modulus, low density, high strength, and excellent biocompatibility. However, the material properties of the titanium used for implants have a higher Young's modulus, which can cause a stress shielding effect. The stress shielding effect occurs because the bone is a living tissue that is constantly modified by bone cells in response to external behavior, and the decrease in mechanical load on the bone due to the stress shielding effect can cause bone resorption (bone loss), implant loosening, and ultimately implant failure [9]. To overcome the stress shielding effect and promote bone-in-growth, the use of porous implant materials is recommended [9]-[10].

Ahmed et al. [11] reported that implants with porous surfaces could stimulate the osseointegration process by increasing the formation of new bone compared to non-porous surfaces. However, the porosity of the porous material and fully porous implant structures are not recommended for implants because they can result in a decrease in mechanical properties and load-bearing requirements. Therefore, a solid core implant combined with a porous material

(hybrid porous dental implant) is recommended for dental implants to ensure that the mechanical properties meet the load-bearing criteria [12].

In a study conducted by Hong Ji-Youn et al. [13], a new method utilizing Metal Injection Molding (MIM) was used to create a porous titanium structure at the apical part of a screw-type implant. A feedstock consisting of a mixture of Titanium Hydride (TiH_2) and a binder was injected into the apical part between the threads of the implant core, which was made using machining methods and CP-titanium grade 4 material. The porous titanium structure created using MIM was able to provide three-dimensional interconnected porosity on the implant surface, which could enhance new bone growth on the surface [13]. The porosity of Ti6Al4V material is influenced by sintering process parameters, including sintering holding time, heating rate, and cooling rate [14].

The aim of this study is to produce a porous titanium alloy material profile made through the process of MIM, which can be applied to the development of a hybrid porous dental implant using titanium alloy as the core material (solid core dental implant). The process parameters employed in this study were sintering time, sintering atmosphere, heating rate, and surface roughness. The surface topography parameters, which encompassed microstructure, porosity, hardness value, and shear strength, of the Ti6Al4V material produced through the MIM and sintering processes under the argon atmosphere were evaluated.

Research Methodology

The material used in this study was Ti6Al4V, referring to ASTM F136 Grade 5 standard, with the chemical composition listed in Table 1.

Table 1: Chemical composition of Ti6Al4V Grade 5

N	C	H	O	Fe	Al	V	Ti
0-0.05	0-0.1	0-0.015	0-0.2	0-0.4	5.5-6.75	3.5-4.5	Balance

Wrought Ti6Al4V specimens with dimensions of 5 x 5 x 3 mm were surface treated with grit P80, P180, and P600. They were then inserted into a cube-shaped mold with dimensions of 5 x 5 x 5 mm, and feedstock Ti6Al4V was injected onto the surface area using MIM. Feedstock Ti6Al4V in this study uses Ryer, Inc. products with the chemical composition listed in Table 2 and binders made of polymers and waxes that must be removed by solvent and thermal debinding processes.

Subsequently, a solvent debinding process was carried out using a hexane solution for 3 hours at a temperature of 60 °C, followed by thermal debinding at 550 °C with a heating rate of 5 °C/minute and a holding time of

60 minutes under an argon atmosphere. The sintering process was carried out at a temperature of 1150 °C for 60 minutes, 90 minutes, and 120 minutes, with an argon atmosphere flow rate of 1 liter/minute. The sintering results were observed and analyzed using a Scanning Electron Microscope (SEM), Energy Dispersive x-ray Spectroscopy (EDS), metallographic observations, hardness, surfcom surface roughness, and shear bond strength tests.

Table 2: Chemical composition of feedstock Ti6Al4V Ryer, Inc.

N	C	H	O	Fe	Al	V	Ti
0.02	0.02	0.006	0.19	0.19	6.22	4.00	88.95

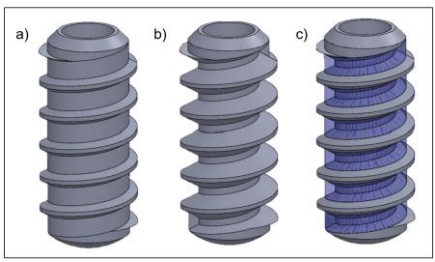

Figure 1: (a) conventional dental, (b) core dental, and (c) hybrid porous dental implant

Figure 1(a) shows a conventional dental implant model. In its development, modifications were made to enhance its porosity. This design development involved creating a core or inner structure for the dental implant capable of accommodating a porous titanium structure from the coronal (top) to the apical (bottom) parts, as depicted in Figure 1(b). Hybrid porous dental implant is engineered to have a porous titanium structure extending from the coronal to the apical regions of the dental implant, as illustrated in Figure 1(c). This aims to facilitate the growth of new bone into the porous titanium structure, thereby maximizing the biomechanical interlocking achieved due to the attachment of new bone while minimizing the effect of stress shielding.

Static loading simulation on the dental implant shaft was conducted using the Fusion 2021 application. The fabrication of the core dental implant was performed using CNC Turning CINCOM A20. Subsequently, the core dental implant underwent a cleaning process to remove machinery lubricants using a mixture of acetone, IPA, and aquadest for 5 minutes. To obtain the surface roughness value of the core dental implant, sandblasting was performed with aluminum oxide F80 using the following parameters: pressure of 0.6 MPa, distance of 20 mm, grit size of 220 µm, blasting duration of 10 seconds, varying rotational speeds of 450/650/750/850/1000/1200 rpm. The

roughness value of the top, flank, and valley areas was measured using Surfcom 9000SD3.

The injection process simulation was performed using SolidWorks Plastics 2020 CAE software with an injection pressure of 3 MPa, a melting temperature of 200 °C, and variations in mold temperature at 180 °C, 190 °C, and 200 °C, as well as variations in the injection gate located at the top, middle, and bottom. After completing the simulation process to find the optimal parameters, the injection process was carried out to produce the green part.

Results and Discussion

The surface topography of the Ti6Al4V alloy material produced by argon sintering at 1150 °C for 60 minutes was evaluated using SEM and EDS. Figure 2 shows the rough surface of the wrought Ti6Al4V material due to the surface treatment. The surface roughness was intended to increase the bond between the wrought and the porous Ti6Al4V materials.

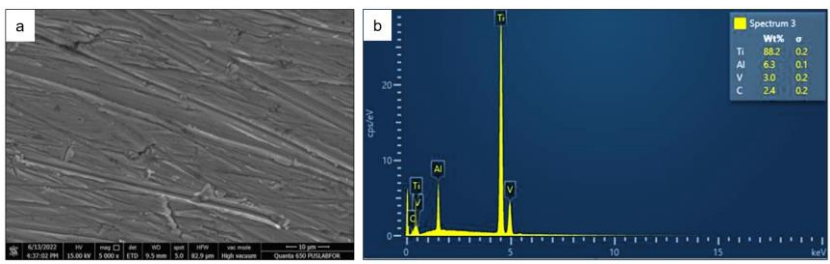

Figure 2: (a) SEM and (b) EDS results of argon sintering of wrought Ti6Al4V material

In Figure 3, the surface structure of the porous material directly bonded to the wrought Ti6Al4V material is shown. Some parts of the surface were still deposited by the polymer binder, so these parts did not reach the final sintering stage. As a result, the polymer binder in these areas was difficult to evaporate and came together with the argon gas flow because it was directly bonded to the wrought Ti6Al4V material. In the EDS results, there was no oxygen element detected in both materials because the sintering process utilized an argon atmosphere to avoid oxidation of the samples.

Based on the microstructure of the sintered porous material, there was much porosity at the grain boundaries (Figures 4(a)-4(c)). This occurred because, during the sintering process, the argon gas was trapped in the pores, preventing the densification process. The presence of porosity in the sample slowed down the grain growth process, resulting in the porosity at the grain

boundaries [15]. There is a significant difference in microstructure between the porous and the wrought materials. As shown in Figures 5(a)-5(c), there is a bonding layer at the interface of Ti6Al4V material sintered the bonding layer is influenced by the polymer on the feedstock and the Ti6Al4V plate material that has been grounded to increase surface roughness, which increases the bonding between the two materials.

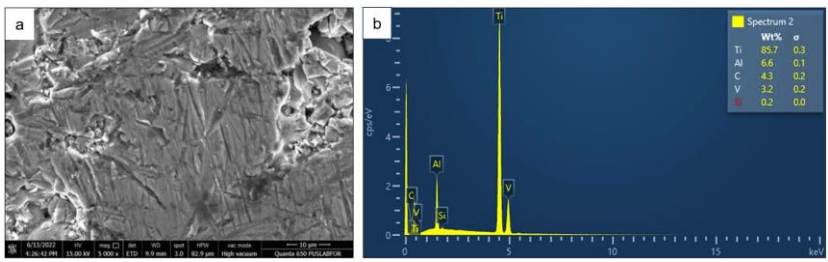

Figure 3: (a) SEM and (b) EDS results of argon sintering of porous Ti6Al4V material

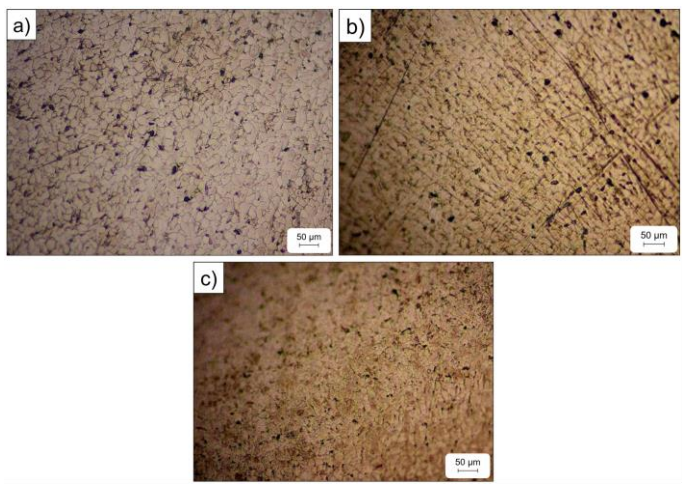

Figure 4: Microstructure of Ti6Al4V porous material sintered at 1150 °C with holding time at (a) 60, (b) 90, and (c) 120 minutes

The microstructure of the porous material tends to form equiaxial grains, while the microstructure of the wrought Ti6Al4V tends to form a lamellar structure, as shown in Figures 6(a)-6(c). The microstructure changes in several stages, starting with the flattening of particle surfaces, the formation of grain boundaries through necking between particles, movement between

particles in open pores, diffusion, and decrease of porosity. Then, the pores shrink between the grain boundaries, the porosity decreases even further, and the grains slowly grow. Finally, the pores close, shrink, and become lodged between the grain boundaries [16].

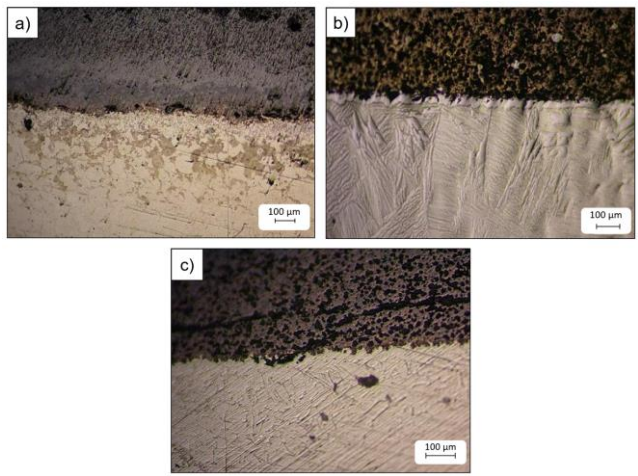

Figure 5: Microstructure of Ti6AL4V interface material sintered at 1150 °C with holding time at (a) 60, (b) 90, and (c) 120 minutes

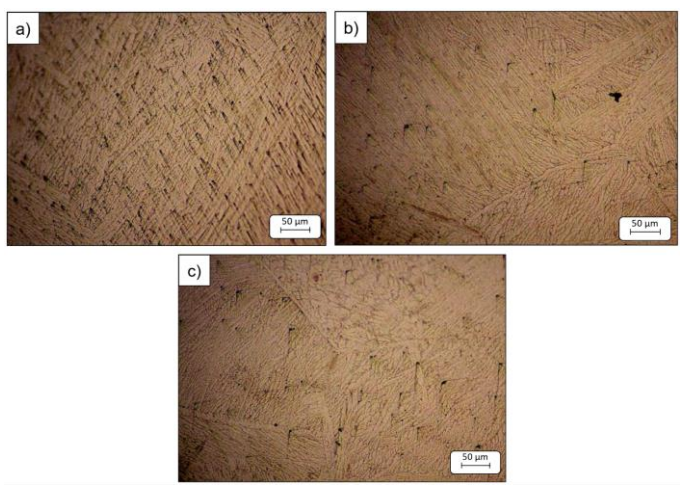

Figure 6: Microstructure of Ti6AL4V wrought material sintered at 1150 °C with holding time at (a) 60, (b) 90, and (c) 120 minutes

Figure 7 shows the percentage of porosity area of the wrought and porous Ti6Al4V materials where the porous Ti6AL4V material has a higher percentage of porosity compared to the wrought Ti6AL4V material. Thus, the mechanical properties of the wrought Ti6AL4V material are greater than those of the porous Ti6AL4V material. The porosity generated in Ti6Al4V material is associated with the holding time of sintering; the higher the holding sintering time, the porosity generated will be more spherical. With the growth of grains along with the increase in the holding time of the sintering process, the pores inside the sample will become round and eventually be closed. The pores will experience significant shrinkage if they come in contact with the α phase. Irregular-shaped porosity is usually found in the β phase matrix.

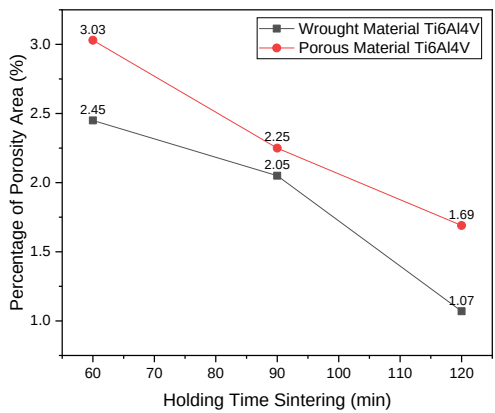

Figure 7: The effect of sintering holding time at 1150 °C on porosity area percentage

In Figure 8, it is shown that at sintering times of 60 and 90 minutes, the porous Ti6Al4V material has lower hardness compared to the wrought material. The lower hardness of the porous Ti6Al4V occurred due to the different microstructure formed in each section, resulting in significant differences in the hardness of the Ti6Al4V material. However, at a sintering time of 120 minutes, the hardness of the wrought material was lower than that of the porous Ti6Al4V material. This phenomenon occurred because of significant grain growth, resulting in a decrease in the hardness of the wrought Ti6Al4V material. At the interface section, the Ti6Al4V material had a higher hardness than the porous Ti6Al4V material at all sintering times. Therefore, the hardness of the wrought, interface, and porous sections will increase with longer sintering times. The increase in hardness is most likely due to the reduction in porosity percentage, which can increase the density, strength, and hardness [17].

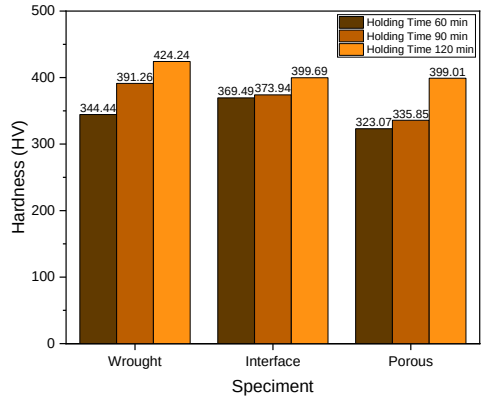

Figure 8: The effect of sintering holding time at 1150 °C on the hardness of Ti6Al4V material

Figure 9 shows the surface roughness value of 2.37 µm following surface treatment using SiC grit P80. As shown in Figure 9, the higher the grit size of the abrasive paper, the lower the surface roughness value. In material bonding, surface treatment greatly affects the level of adhesion. The higher the surface roughness value, the higher the bonding strength at the joint. However, the bonding strength of the joint will decrease when it exceeds the optimum limit of surface roughness. In line with this, Budhe et al. [18] found that the optimum surface roughness (*Ra*) values to increase the bonding strength were in the range of 1.75-2.5 µm. Meanwhile, if the surface roughness values were in the range of 2.5-4.1 µm, the bonding strength tended to decrease.

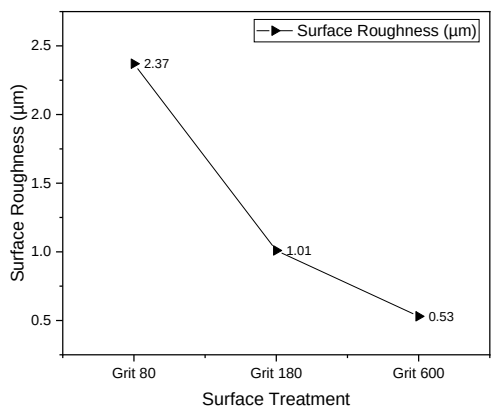

Figure 9: Surface roughness of Ti6Al4V material after surface treatment with SiC grit sandpaper of P80, P180, and P600

Surface treatment with grit P80 resulted in the highest shear stress value of 1.54 MPa (Figure 10). The shear stress result of grit P180 was similar to grit P80. Interestingly, the shear stress result of grit P600 decreased due to the low value of surface roughness obtained from the surface treatment. Grinding removes contaminants that cause a decrease in surface bonding, leading to poor bonding strength and low shear stress. Additionally, the grinding process can also remove the oxide layer formed on the surface [19]-[21].

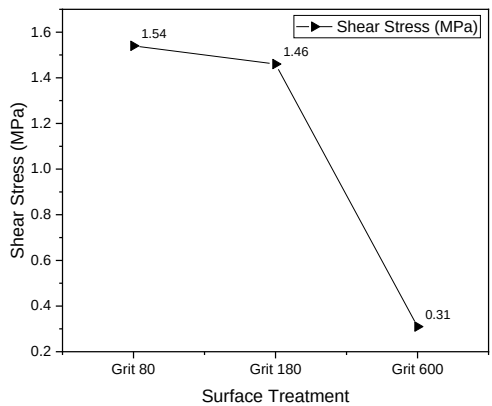

Figure 10: Result of shear bond strength test

Figure 11 illustrates the macroscopic photo of the wrought and porous Ti6Al4V materials contour surface, showing the tendency of both materials to bond at the edge. Meanwhile, the middle part of the porous Ti6Al4V material experienced shrinkage after sintering, making it difficult to bond with the bottom part of the wrought Ti6Al4V material.

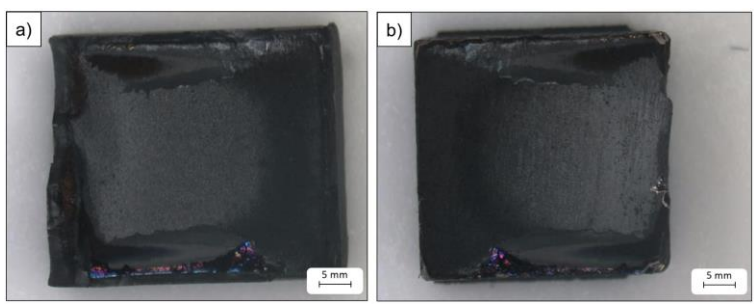

Figure 11: (a) Porous and (b) wrought Ti6Al4V materials after shear bond strength testing

The development of combining implant materials with porous materials can be applied to create a hybrid porous dental implant by adding porous material that fills the thread surface. The simulation results of static loading of the porous part of the hybrid porous dental implant showed no mechanical failure (Figure 12). This result was achieved because the stress value did not exceed the yield strength value of the porous material, which was 1.58 MPa. Furthermore, the Ti6Al4V porous material with a porosity percentage of 75% had a yield strength value of 79.21 MPa, which is safe to use in the hybrid porous dental implant system.

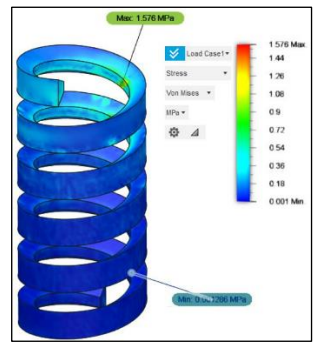

Figure 12: Simulation results of static loading of porous parts

As shown in Figure 13, the result of the dental implant core sandblasting process has a dark color. The dark color formed due to residual lubricant originating from the machining process, causing a carbon oxidation reaction on the surface of the heated dental implant during the sandblasting process [22].

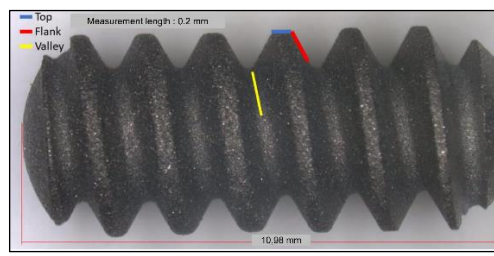

Figure 13: Surface roughness measurement area after sandblasting and cleaning process

Figure 14 shows the effect of rotational speed on surface roughness, which is not significant. However, the highest surface roughness value was

obtained from the rotational speed parameters of 650 and 750 rpm. Then, using the Material Removal Rate (MRR) formula, which calculates the rate of material removal per unit time on the workpiece, the highest MRR value was obtained at a rotation speed of 750 rpm.

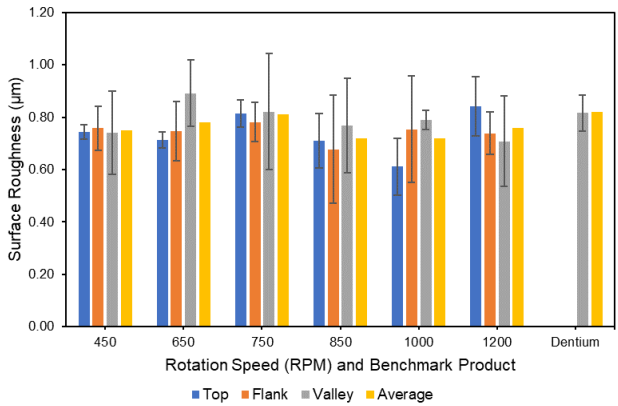

Figure 14: Results of the effect of rotation speed on roughness values on the top, flank, and valley areas

The simulation results of the injection from the top gate in Figure 15 suggest that the recommended injection parameter is a mold temperature of 200 °C. At mold temperatures of 180 °C and 190 °C, the feedstock flow was unable to fill the cavity due to hardening (short shot).

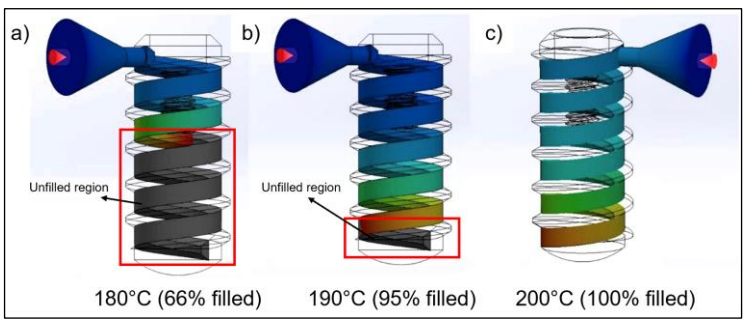

Figure 15: Simulation results of injection from the top gate with a mold temperature of (a) 180 °C, (b) 190 °C, and (c) 200 °C

The injection results from the middle gate in Figure 16 indicate that the optimal parameter is obtained at mold temperatures of 190 °C and 200 °C. Meanwhile, at a mold temperature of 180 °C, the feedstock flow did not fill

the cavity and underwent hardening (a short shot). The injection parameters with the middle gate location are the best recommendation based on simulation results that show the ability of the feedstock to fill the mold with a temperature not exceeding 200 °C. Therefore, these parameters were further used in the injection process.

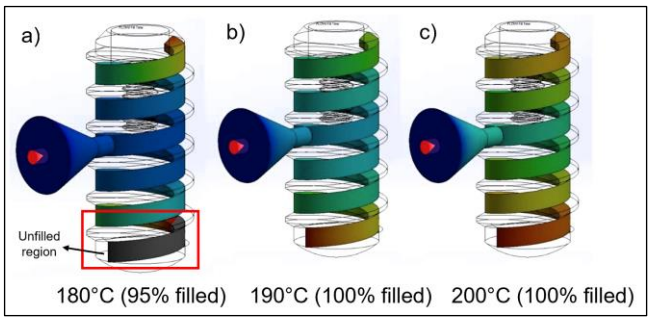

Figure 16: Simulation results of injection from the middle gate with a mold temperature of (a) 180 °C, b) 190 °C, and c) 200 °C

The simulation results in Figure 17 show that the recommended mold temperature of the injection parameter from the bottom gate is 200 °C. On the other hand, at temperatures of 180 °C and 190 °C, the feedstock flow did not fully fill the cavity due to hardening (short shot).

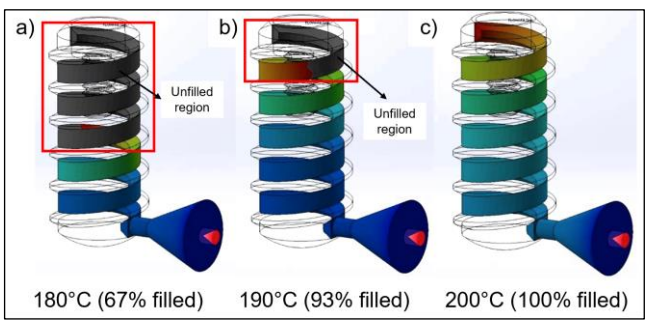

Figure 17: Simulation results of injection from the bottom gate with a mold temperature of (a) 180 °C, (b) 190 °C, and (c) 200 °C

Based on the microscopic observation of injection results at three different mold temperatures, the porous material was successfully injected and filled the entire cavity area where the best result was obtained at 180 °C (Figure 18(a)). Meanwhile, the injection results at mold temperatures of 190 °C and

200 °C showed parts of the porous material that were detached from the mold, as shown in Figures 18(b)-18(c).

In Figure 19, the CAD design shows that the dental implant core and the green part of the porous material had a volume of 124.65 and 19.72 mm³, respectively. The density of Ti6Al4V grade 5 was 4.43 g/cc, while the density of the green part feedstock, based on RYER's datasheet, was 3.03 g/cc. Thus, the mass of the green part hybrid porous dental implant was obtained by multiplying the volume and density of the material. Based on the calculation, the highest injection mass was obtained at a mold temperature of 180 °C, which was 202% of the green part design mass.

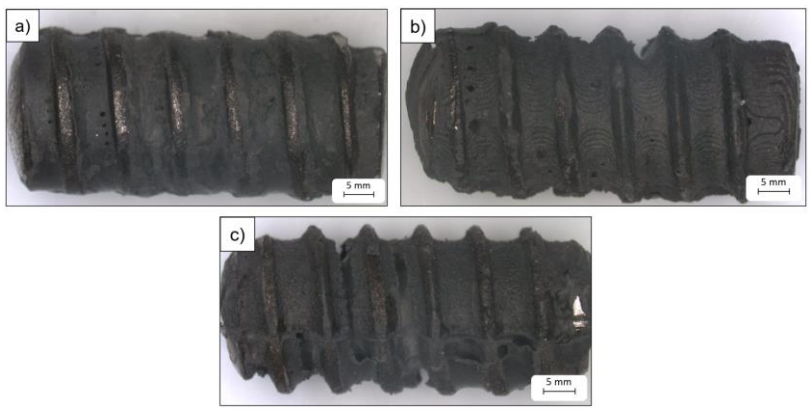

Figure 18: Microscopic results of the green part with a mold temperature of (a) 180 °C, (b) 190 °C, and (c) 200 °C

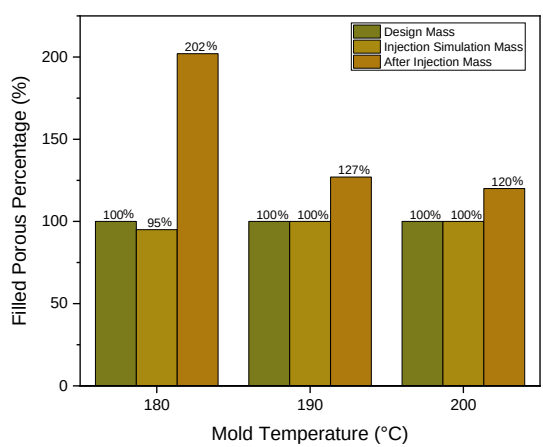

Figure 19: Comparison of porous design mass with green part mass

Conclusion

There are several conclusions taken from this research, namely:

1. Ti6Al4V material produced by MIM consists of porous and wrought materials that adhere to each other. After passing through the sintering process at a temperature of 1150 °C with variations in holding time of 60, 90, and 120 minutes, the two materials produce different microstructures. The porous material produces an equiaxed microstructure with α and β phases, while the wrought material produces a lamellar microstructure with α and β phases.
2. By varying the surface roughness of *Ra* 2.37 μm, 1.01 μm, and 0.54 μm to increase the bonding strength between the wrought and the porous Ti6Al4V materials, the shear stress increases as the material surface becomes rougher, especially when polished with grit P80.
3. Sandblasting with a pressure parameter of 0.6 MPa, a shooting distance of 20 mm, a grit size of 220 μm (F80), and a blasting duration of 10 seconds with variations in the rotation speed of 450-1200 RPM is the recommended parameter to achieve a surface roughness of *Ra* 0.72-0.80 μm.
4. Based on simulation and experimental results, the gate in the middle of the cavity is the recommended injection location. The best injection parameters based on the MIM process of the green part in the production of a hybrid porous dental implant are a melting temperature of 200 °C, a mold temperature of 180 °C, and an injection pressure of 3.6 MPa.

Contribution of Authors

S. S.: Conceptualization, Supervision; A. W. W.: Writing – original draft, Visualization; M. F. Z.: Conceptualization, Methodology, Experimental, Visualization. D. J.: Conceptualization, Methodology, Experimental, Visualization. All authors reviewed and approved the final version of this work.

Funding

This work is supported by PTUPT Grants contract number NKB-878/UN2.RST/HKP.05.00/2022.

Conflict of Interest

All authors declare that they have no conflicts of interest.

Acknowledgment

This research was supported by the TiBio Laboratory of the Faculty of Engineering, University of Indonesia. The authors would like to acknowledge the Department of Mechanical Engineering and the Department of Metallurgical and Materials Engineering, University of Indonesia for providing the facilities to conduct this research.

References

[1] K. Lovera-Prado, V. Vanaclocha, C. M. Atienza, A. Vanaclocha, P. Jordá-Gómez, N. Saiz-Sapena, and L. Vanaclocha, "Barbed dental Ti6Al4V alloy screw: design and bench testing", *Materials,* vol. 16, no. 6, pp. 1-13, 2023. https://doi.org/10.3390/ma16062228

[2] K. J. Ferro, "The glossary of prosthodontic terms: Ninth edition," *Journal of Prosthetic Dentistry*, vol. 117, no. 5, pp. 1–105, 2017. doi: 10.1016/j.prosdent.2016.12.001

[3] F. Javed, H. B. Ahmed, R. Crespi, and G. E. Romanos, "Role of primary stability for successful osseointegration of dental implants: Factors of influence and evaluation", *Interventional Medicine and Applied Science,* vol. 5, no. 4, pp. 162-167, 2013. https://doi.org/ 10.1556/IMAS.5.2013.4.3

[4] M. Akoğlan, U. Tatli, C. Kurtoğlu, F. Salimov, and M. Kürkçü, "M. Akoğlan, U. Tatli, C. Kurtoğlu, F. Salimov, and M. Kürkçü, "Effects of different loading protocols on the secondary stability and peri-implant bone density of the single implants in the posterior maxilla", *Clinical Implant Dentistry and Related Research,* vol. 19, no. 4, pp. 624-631, 2017. https://doi.org/10.1111/cid.12492

[5] B. Chrcanovic, T. Albrektsson, and A. Wennerberg, "Reasons for failures of oral implants," *Journal of Oral Rehabilitation,* vol. 41, no. 6, pp. 443-476, 2014. https://doi.org/10.1111/joor.12157

[6] R. Smeets, B. Stadlinger, F. Schwarz, B. Beck-Broichsitter, O. Jung, C. Precht, F. Kloss, A. Gröbe, M. Heiland, and T. Ebker, "Impact of dental implant surface modifications on osseointegration", *BioMed Research International,* vol. 2016, pp. 1-16, 2016. https://doi.org/10.1155/2016/6285620

[7] L. Le Guéhennec, A. Soueidan, P. Layrolle, and Y. Amouriq, "Surface treatments of titanium dental implants for rapid osseointegration", *Dental Materials,* vol. 23, no. 7, pp. 844-854, 2007. https://doi.org/10.1016/j.dental.2006.06.025

[8] P. G. Coelho, R. Jimbo, N. Tovar, and E. A. Bonfante, "Osseointegration: Hierarchical designing encompassing the macrometer, micrometer, and nanometer length scales", *Dental Materials,* vol. 31, no. 1, pp. 37-52, 2015. https://doi.org/10.1016/j.dental.2014.10.007

[9] B. V. Krishna, S. Bose, and A. Bandyopadhyay, "Low stiffness porous Ti structures for load-bearing implants", *Acta Biomaterialia,* vol. 3, no. 6, pp. 997-1006, 2007. https://doi.org/10.1016/j.actbio.2007.03.008

[10] Z. J. Wally, W. Van Grunsven, F. Claeyssens, R. Goodall, and G. C. Reilly, "Porous titanium for dental implant applications", *Metals,* vol. 5, no. 4, pp. 1902-1920, 2015. https://doi.org/10.3390/met5041902

[11] A. Ahmed, A. Al-Rasheed, M. Badwelan, and H. S. Alghamdi, "Peri-Implant bone response around porous-surface dental implants: A preclinical meta-analysis," *The Saudi Dental Journal,* vol. 33, no. 5, pp. 239-247, 2021. https://doi.org/10.1016/j.sdentj.2020.12.006

[12] G. Ryan, A. Pandit, and D. P. Apatsidis, "Fabrication methods of porous metals for use in orthopaedic applications", *Biomaterials,* vol. 27, no. 13, pp. 2651-2670, 2006. https://doi.org/ 10.1016/j.biomaterials.2005.12.002

[13] J. Y. Hong, S. Y. Ko, W. Lee, Y. Y. Chang, S. H. Kim, and J. H. Yun, "Enhancement of bone ingrowth into a porous titanium structure to improve osseointegration of dental implants: a pilot study in the canine model", *Materials,* vol. 13, no. 14, pp. 1-13, 2020. https://doi.org/ 10.3390/ma13143061

[14] N. H. Mohamad Nor, H. Nor Hafiez, and M. A. Yahaya, "Optimizing sintering process to produce highest density of porous Ti-6Al-4V," *Journal of Mechanical Engineering*, no. 6, pp. 44-55, 2018.

[15] C. Ji, N. Loh, K. Khor, and S. Tor, "Sintering study of 316L stainless steel metal injection molding parts using Taguchi method: Final density", *Materials Science and Engineering: A,* vol. 311, no. 1-2, pp. 74-82, 2001. [Online]. Available: www.elsevier.com/locate/msea.

[16] Y. Xu, K. Zhang, L. Fu, T. Tong, L. Cao, Q. Zhang, and L. Chen, "Effect of MgO addition on sintering temperature, crystal structure, dielectric and ferroelectric properties of lead-free BZT ceramics," *Journal of Materials Science: Materials in Electronics,* vol. 30, pp. 7582-7589, 2019. https://doi.org/10.1007/s10854-019-01073-x

[17] Y. Pan, H. Li, Y. Liu, Y. Liu, K. Hu, N. Wang, Z. Lu, J. Liang, and S. He, "Effect of holding time during sintering on microstructure and properties of 3D printed alumina ceramics", *Frontiers in Materials,* vol. 7, pp. 1-12, 2020. https://doi.org/10.3389/fmats.2020.00054

[18] S. Budhe, A. Ghumatkar, N. Birajdar, and M. Banea, “Effect of surface roughness using different adherend materials on the adhesive bond strength”, *Applied Adhesion Science,* vol. 3, pp. 1-10, 2015. https://doi.org/10.1186/s40563-015- 0050-4

[19] V. P. Nguyen, T. N. Dang, C. C. Le, and D. A. Wang, “Effect of coating thickness on fatigue behavior of AISI 1045 steel with HVOF thermal spray and hard chrome electroplating,” *Journal of Thermal Spray Technology,* vol. 29, no. 8, pp. 1968-1981, 2020. https://doi.org/10.1007/s11666-020-01090-x

[20] B. S. Lim, S. M. Heo, Y. K. Lee, and C. W. Kim, “Shear bond strength between titanium alloys and composite resin: Sandblasting versus fluoride-gel treatment,” *Journal of Biomedical Materials Research Part B: Applied Biomaterials: An Official Journal of The Society for Biomaterials, The Japanese Society for Biomaterials, and The Australian Society for Biomaterials and The Korean Society for Biomaterials,* vol. 64, no. 1, pp. 38-43, 2003. https://doi.org/ 10.1002/jbm.b.10484

[21] M. B. Donmez, G. Çakmak, D. Yılmaz, M. Schimmel, S. Abou-Ayash, B. Yilmaz, and A. Peutzfeldt, “Bond strength of additively manufactured composite resins to dentin and titanium when bonded with dual-polymerizing resin cements,” *The Journal of Prosthetic Dentistry*, 2023. https://doi.org/ 10.1016/j.prosdent.2023.04.003

[22] D. Gross, A. Heinz, S. Amon, T. Meier, R. Schmand, and N. Hanenkamp, “Investigation of carbon dioxide based blasting technologies as cryogenic deburring method for titanium alloy and stainless steel”, *Applied Mechanics and Materials*, vol. 882, pp. 142-153, 2018. https://doi.org/ 10.4028/www.scientific.net/AMM.882.142